International Journal of Mass Spectrometry 302 (2011) 59–68

Contents lists available at ScienceDirect

International Journal of Mass Spectrometry

journal homepage: www.elsevier.com/locate/ijms

Methods for the analysis of high precision differential hydrogen–deuterium exchange data

Michael J. Chalmers[a,b], Bruce D. Pascal[c], Scooter Willis[c], Jun Zhang[a], Stephen J. Iturria[d], Jeffery A. Dodge[d], Patrick R. Griffin[a,b,*]

[a] Department of Molecular Therapeutics, The Scripps Research Institute, Scripps Florida, 130 Scripps Way, Jupiter, FL 33458, United States
[b] The Scripps Research Molecular Screening Center, The Scripps Research Institute, Scripps Florida, 130 Scripps Way, Jupiter, FL 33458, United States
[c] Translational Research Institute, Informatics, The Scripps Research Institute, Scripps Florida, 130 Scripps Way, Jupiter, FL 33458, United States
[d] Lilly Research Laboratories, Eli Lilly and Company, Indianapolis, IN 46285, United States

ARTICLE INFO

Article history:
Received 20 May 2010
Received in revised form 16 July 2010
Accepted 2 August 2010
Available online 10 August 2010

Keywords:
HDX
MS
Ligand
Screening
Nuclear receptor

ABSTRACT

Hydrogen/deuterium exchange (HDX) mass spectrometry has been widely applied to the characterization of protein dynamics. More recently, differential HDX has been shown to be effective for the characterization of ligand binding. Previously we have described a fully automated HDX system for use as a ligand screening platform. Here we describe and validate the required data analysis workflow to facilitate the use of HDX as a robust approach for ligand screening. Following acquisition of HDX data at a single on-exchange time point ($n \geq 3$), one way analysis of variance in conjunction with the Tukey multiple comparison procedure is used to establish the significance of any measured difference. Analysis results are graphed with respect to a single peptide, ligand or group of ligands, or displayed as an overview within a heat map. For the heat map display, only Δ%D values with a Tukey-adjusted *P*-value less than 0.05 are colored. Hierarchical clustering is used to bin compounds with highly similar HDX signatures. The workflow is evaluated with a small dataset showing the ligand binding domain (LDB) of the nuclear receptor peroxisome proliferator-activated receptor gamma (PPARγ) screened against 10 functionally selective ligands. More significantly, data for the vitamin D receptor (VDR) in complex with 87 ligands are presented. To highlight the robustness and precision of our automated HDX platform we analyzed the data from 4191 replicate HDX measurements acquired over an eight month timeframe. Ninety six percent of these measurements were within 10% of the mean value. Work has begun to integrate these analysis and graphing components within our HDX software suite.

1. Introduction

Hydrogen/deuterium exchange (HDX) in combination with mass spectrometry (MS) [1–5] is a powerful method for the characterization of protein dynamics [6–10]. The technique has been applied to determine changes in dynamics (differential HDX) between a protein and its binding partners [11]. These binding partners have included proteins, peptides, DNA, RNA, small molecules [12–22], or combinations of all five [23]. HDX has found use as an approach to guide construct design in X-ray crystallography methods development [24,25] and has been applied to challenging molecules such as antibodies [10] and membrane proteins [26–30].

Many of these experiments report HDX results from differential analysis between two states of a protein, for example HDX of a protein ± ligand. Our group has advocated the use of automation [13,31] to reduce random, gross and systematic errors during data acquisition [14]. Following acquisition, the percent deuterium values must be extracted from the MS spectra, and the correlated data volume can be considerable. For example, a single differential HDX experiment may contain 100 peptides. Four replicate analyses of seven on-exchange time points will yield 5600 data points. Screening just 50 ligands will expand that dataset to 280,000 values. The data generated from a single research group over just a few years can quickly top a million data points, all of which require tools for visualization and protocols for quality control, archiving and data backup. More importantly, approaches to provide significance of changes on large datasets are needed.

Significant effort has been dedicated to software tools for the analysis of HDX data [31–40]; however the majority of published software are focused upon the generation of percent deuterium values and not downstream data analysis. Some applications contain

* Corresponding author at: Department of Molecular Therapeutics, The Scripps Research Institute, Scripps Florida, 130 Scripps Way, Jupiter, FL 33458, United States. Tel.: +1 561 228 2200; fax: +1 561 228 3081.
E-mail address: pgriffin@scripps.edu (P.R. Griffin).

1387-3806/$ – see front matter © 2010 Elsevier B.V. All rights reserved.
doi:10.1016/j.ijms.2010.08.002

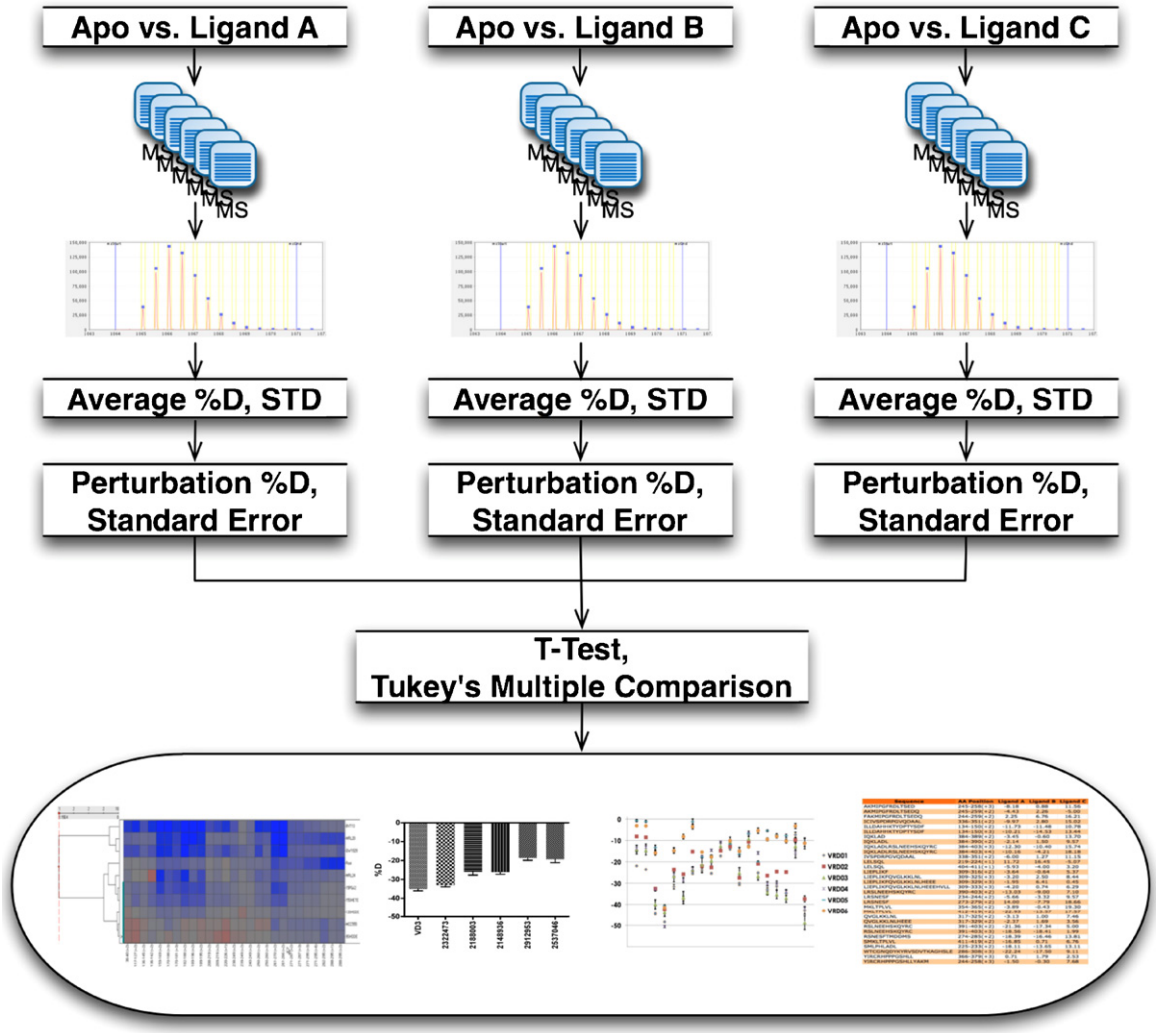

Fig. 1. Schematic representation of our differential HDX data analysis workflow.

no graphing components and others contain useful, but somewhat limited, display elements such as the ability to compare two datasets. The need therefore remains for a software solution that is capable of the cross comparison of multiple (>50) datasets acquired over a significant time period by multiple users. Such a software package will complete our goal of producing a HDX platform that is comprehensive, rapid, and robust enough for use in screening applications. In this context we are interested in developing methods for screening functionally selective nuclear receptor modulators; however, the approach can be applied to other target proteins such as kinases or G-protein coupled receptors (GPCRs).

Our approach to HDX software development has been to store all the relevant MS spectral data and HDX results in a relational database and is unique in this regard [35]. Unlike a standalone application, this structure is ideal for HDX screening applications that require the cross comparison of multiple datasets. The database also provides a single storage point for all data generated within the laboratory and allows for easy sharing of data between members of a laboratory. Critically, the database provides a single target for data archiving. Quality control for processed data is also possible. For example, any project can be queried to provide the standard deviation of all measurements. At the time of writing there were 1,334,978 HDX values and associated MS spectra stored within our database (active since April 2008, not including values in the external user database). All of these data points and spectra may be accessed directly from any web browser. This amount of data would impossible to manage across multiple users with the current generation of standalone HDX software applications.

We have previously published the differential HDX data for PPARγ LBD in complex with 10 ligands of interest at single time point [14]. During the evaluation of this dataset we determined statistical significance between apo (ligand free) receptor and ligand bound receptor with a two tailed t-test. Although this approach allowed for the determination of peptides that are different from apo receptor, we did not address a crucial question; what is the statistical significance of the changes observed between those 10 ligands? We understand that both ligand "A" and "B" differ from "apo" for a particular peptide, however is "A" different from "B"? To answer these questions we have chosen to re-evaluate the aforementioned dataset. In doing so, we seek to establish a validated workflow for HDX screening data that will subsequently be integrated into our HDX software. This workflow was then applied to a large VDR HDX dataset (>20,000 %D values) obtained for analysis of the receptor in complex with 87 ligands, including small molecules, cofactor proteins and DNA.

2. Materials and methods

PPARγ LBD was expressed and purified as described previously [12,14]. His-hVDR ligand binding domain (residues 118–425,

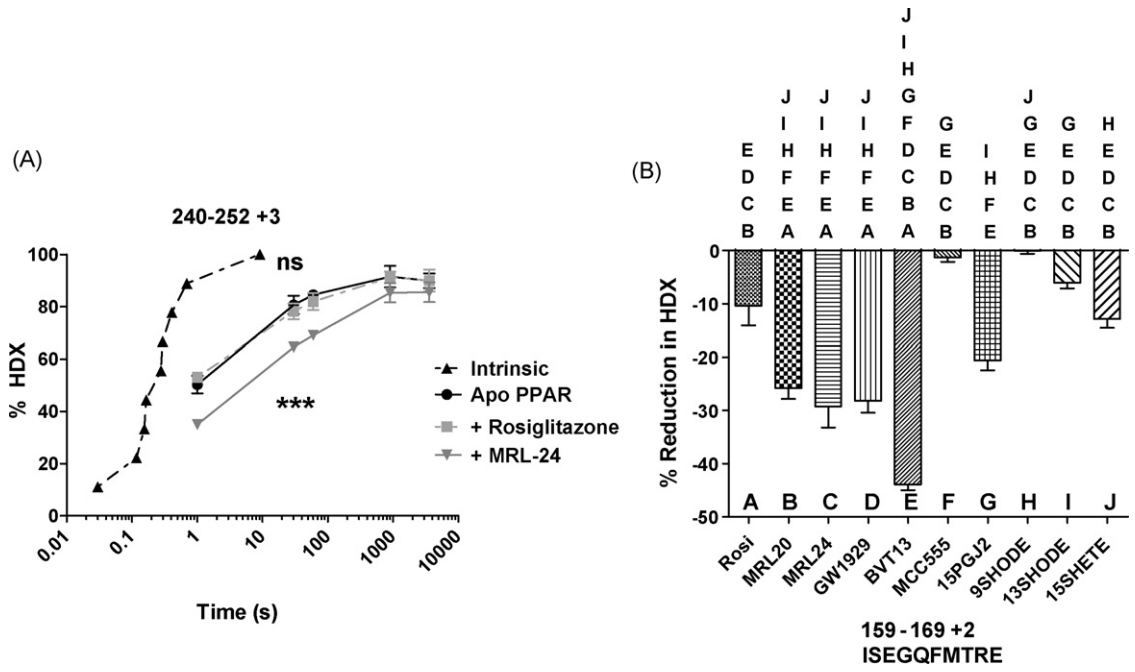

Fig. 2. (A) HDX data for PPARγ LBD in complex with full agonist rosiglitazone and the partial agonist MRL-24. A two tailed *t*-test of the 30 s data showed no significant difference between ligand free PPAR (apo) and the rosiglitazone bound receptor. In contrast, a significant reduction in exchange was observed following binding of MRL-24. It should be noted that each differential HDX experiment contains its own "apo" internal control. For clarity, only the apo data associated with the rosiglitazone are displayed. There was complete overlap between the two apo samples (see text for a discussion on the repeatability of our automated platform for data acquisition). Fig. 1(B). Differential HDX data for the PPARγ beta sheet region 159–169 ($[M+2H]^{2+}$ ion) following 30 s of exchange. Data are shown for 10 ligands of interest. The chart is annotated with the results from the Tukey multiple comparison test. The letters above each bar represent those ligands that exhibit a significant difference with a *P*-value < 0.05. For example, A(rosi) is significantly different from B, C, D and E.

Δ[165–215]) was expressed in *E. coli* BL21 cells as inclusion bodies. Inclusion bodies were solubilized in a guanidine–HCL buffer, captured by Ni–NTA, refolded by dialysis and purified on Q Sepharose FastFlow (QFF) chromatography. The final protein buffer was 20 mM Hepes (pH 7.5), 150 mM NaCl, 10 mM methionine, 10% glycerol, 5 mM DTT. Full length WT His-hVDR and WT Flag-hRXRα were expressed in Baculovirus system and purified by Ni–NTA/SEC or Flag/SEC, respectively, as described previously [41].

HDX mass spectrometry was performed with a fully automated system as described previously [13,14,31]. Briefly, a CTC Twin PAL liquid handling robot (LEAP Technologies, Carborro, NC) was interfaced with either a linear ion trap mass or orbitrap mass spectrometer (LTQ & Exactive, respectively, Thermo Electron, San Jose, CA). 4 μL of protein solution was diluted to 20 μL with D_2O buffer. Following on-exchange, the reaction was quenched with a cold 3 M urea solution containing 1% TFA. The sample was then passed over an immobilized pepsin column (prepared in house), desalted with a C_8 sample trap (1 mm × 10 mm; Thermo Fisher Hypersil gold) and eluted across a C_{18} HPLC (1 mm × 50 mm; Thermo Fisher Hypersil gold) column into the ESI source of the mass spectrometer. All HDX values are the average of three or four individual on-exchange experiments acquired in a random order.

HDX data analysis was performed with an updated version of our HDX software platform [35,36]. Statistical tests were performed with Prism v5.0 (Graphpad Software, CA) and in custom software with the Apache Commons Mathematics Library. Hierarchical clustering was performed with SpotFire Decisionsite v9.1 for functional genomics (TIBCO, Palo Alto, CA). For HCA data were clustered according to Wards method [43].

3. Results and discussion

In this work we establish a workflow for the analysis of differential HDX data that is compatible with large datasets. The complete experimental workflow is shown in Fig. 1 and the individual components of the scheme are described and evaluated in detail below.

3.1. HDX screening dataset

We have previously shown that single time point differential HDX data can provide rapid discriminatory information between multiple synthetic and endogenous PPARγ ligands [14]. To illustrate this approach, Fig. 2(A) shows that a reduction in exchange was observed for PPARγ-LBD residues 240–252 ($[M+3H]^{3+}$) following binding of the partial agonist MRL-24, but not full agonist rosiglitazone. The results from a two tailed *t*-test of the 30 s data show that rosiglitazone is not significantly different from apo receptor while the *P*-value for the MRL-24 data was <0.0001 ($n = 4$). For this region of the receptor, the distinction between rosiglitazone and MRL24 can be made from the 30 s exchange data, and therefore a complete differential HDX dataset is not required to distinguish between these two functionally selective ligands. We have demonstrated that ligand discrimination at the 30 s time point is possible for all regions of PPARγ contained within the dataset and as such acquisition and analysis of a complete HDX dataset is not required to differentiate functionally selective PPARγ modulators. For additional details and supporting data pertaining to the single time point HDX method we direct the reader to our recent publication [14]. We do acknowledge the possibility that certain ligands may exhibit significant changes in HDX behavior which are not reflected to statistical significance in the 30 s data. Regardless, this does not diminish the validity of information obtained from the 30 s HDX dataset.

To establish a robust data analysis workflow for future HDX screening efforts we have revisited a differential HDX dataset obtained for PPARγ LBD in complex with 10 ligands of interest [14]. The complete dataset is shown in Table 1. The mean percent change

Table 1
HDX screening data for PPARγ LBD with synthetic, and endogenous, ligands.

Peptide	Rosi	MRL20	MRL24	GW1929	BVT13	MCC555	15PGJ2	9SHODE	13SHODE	15SHETE
30–40 (+2)	−1 (2)	−9 (0)	−3 (3)	−16 (1)	−22 (1)	3 (1)	−4 (4)	4 (2)	1 (1)	−2 (2)
97–105 (+2)	−30 (19)	−66 (3)	−51 (2)	−42 (3)	−63 (0)	−3 (2)	NaN	−7 (4)	−6 (3)	−11 (1)
117–127 (+2)	−1 (2)	−7 (3)	0 (5)	−17 (3)	−29 (1)	4 (1)	−6 (4)	5 (2)	−1 (2)	−8 (5)
136–145 (+2)	−2 (2)	−6 (0)	0 (2)	−9 (1)	−14 (0)	2 (2)	−4 (2)	1 (2)	−2 (1)	−4 (3)
136–142 (+2)	−3 (5)	−7 (2)	7 (5)	−14 (1)	−26 (1)	−1 (1)	−8 (4)	−2 (2)	−3 (1)	−9 (3)
159–169 (+2)	−10 (7)	−26 (4)	−29 (8)	−28 (5)	−44 (2)	−1 (1)	−21 (4)	0 (1)	−6 (2)	−13 (3)
170–188 (+3)	−10 (6)	−25 (3)	−14 (5)	−26 (3)	−34 (1)	−5 (1)	−13 (3)	1 (3)	−6 (2)	−11 (5)
170–181 (+3)	−10 (5)	−19 (1)	−18 (7)	−18 (6)	−26 (2)	−2 (0)	−16 (2)	−1 (2)	−4 (2)	−10 (2)
182–188 (+2)	−8 (14)	−37 (4)	−29 (2)	−34 (4)	−46 (0)	2 (2)	−19 (6)	1 (4)	−7 (3)	−16 (8)
189–196 (+2)	−6 (9)	−31 (1)	−9 (3)	−22 (1)	−36 (1)	1 (1)	−16 (4)	0 (2)	−5 (2)	−13 (6)
189–195 (+2)	−7 (9)	−26 (1)	−17 (2)	−24 (2)	−40 (1)	2 (2)	−18 (4)	2 (3)	−6 (3)	−14 (8)
208–219 (+2)	−1 (1)	−4 (2)	−2 (3)	−8 (4)	−16 (1)	1 (0)	−5 (2)	1 (2)	−1 (1)	−5 (3)
209–219 (+2)	−3 (2)	−5 (3)	−3 (4)	−11 (5)	−20 (1)	1 (1)	−6 (2)	4 (2)	−1 (1)	−6 (4)
220–226 (+1)	1 (1)	−6 (1)	0 (8)	−17 (7)	−25 (2)	4 (1)	−5 (5)	6 (2)	0 (2)	−6 (4)
238–249 (+2)	−4 (3)	−6 (3)	−4 (9)	−11 (7)	−14 (3)	0 (2)	−3 (4)	2 (1)	−1 (2)	−4 (1)
239–249 (+2)	−3 (3)	−2 (2)	−1 (7)	−7 (7)	−2 (3)	1 (2)	−1 (3)	2 (1)	3 (2)	−2 (1)
240–249 (+2)	−5 (5)	−6 (3)	−4 (9)	−6 (9)	−6 (4)	−1 (3)	−2 (3)	0 (1)	0 (3)	−2 (2)
250–260 (+2)	−5 (3)	−13 (3)	−9 (7)	−19 (6)	−28 (2)	2 (1)	−6 (2)	0 (2)	−2 (1)	−6 (2)
250–260 (+3)	−5 (3)	−10 (3)	−7 (5)	−8 (4)	−25 (2)	2 (1)	−6 (2)	0 (1)	−2 (1)	−7 (3)
261–270 (+2)	−18 (15)	−32 (2)	−13 (3)	−28 (4)	−33 (2)	−9 (1)	−20 (3)	−3 (2)	−5 (2)	−13 (4)
261–266 (+2)	−13 (12)	−33 (3)	−9 (5)	−31 (2)	−36 (2)	−3 (1)	−18 (4)	−3 (1)	−5 (1)	−14 (5)
271–287 (+2)	−12 (6)	−13 (3)	−7 (8)	−9 (5)	−11 (4)	−5 (3)	−7 (3)	−3 (2)	−2 (3)	−4 (2)
271–287 (+3)	−12 (6)	−13 (3)	−7 (7)	−9 (5)	−11 (4)	−5 (3)	−6 (3)	−3 (2)	−2 (3)	−4 (2)
271–295 (+3)	−16 (8)	−14 (3)	−7 (7)	−8 (4)	−8 (5)	−5 (3)	−5 (3)	−3 (3)	−2 (3)	−3 (3)
271–295 (+4)	−16 (8)	−15 (3)	−6 (8)	−9 (4)	−7 (5)	−5 (3)	−5 (3)	−3 (3)	−2 (3)	−3 (3)
282–295 (+2)	−25 (13)	−18 (2)	−7 (9)	−8 (4)	−5 (7)	−9 (7)	−2 (3)	−8 (4)	−1 (6)	−2 (4)
288–295 (+1)	−28 (14)	−19 (2)	−5 (11)	−7 (5)	−5 (6)	−4 (3)	−2 (3)	−3 (4)	−1 (4)	−2 (3)
288–295 (+2)	−29 (15)	−18 (2)	−5 (12)	−10 (5)	−5 (7)	−5 (3)	−2 (3)	−4 (5)	−1 (5)	−2 (4)

($n = 4$) in HDX kinetics (and standard deviation) for each region (peptide start-end (z)) of the receptor is shown for all ligands. A negative number indicates that the measured %D (30 s on-exchange) for the ligand bound receptor was less than the measured %D for the unliganded apo receptor.

A bar chart representing the 30 s HDX data for the 159–169 $[M+2H]^{2+}$ peptide is shown in Fig. 2(B). These data are plotted as the difference in HDX rate from the apo receptor for 10 PPARγ ligands. It should be noted that the HDX data for each ligand was acquired in a random order with its own internal "apo" or receptor only plus DMSO control [13,14]. Although the internal control requires an increase in data acquisition and analysis time, the use of a control ensures that the precision of the experiment is minimally impacted by changes in environmental or experimental conditions such as pH, temperature, and chromatographic retention time. The acquisition of data in this fashion allows data acquired over many days, or even months to years to be compared (see Section 3.4 for more details).

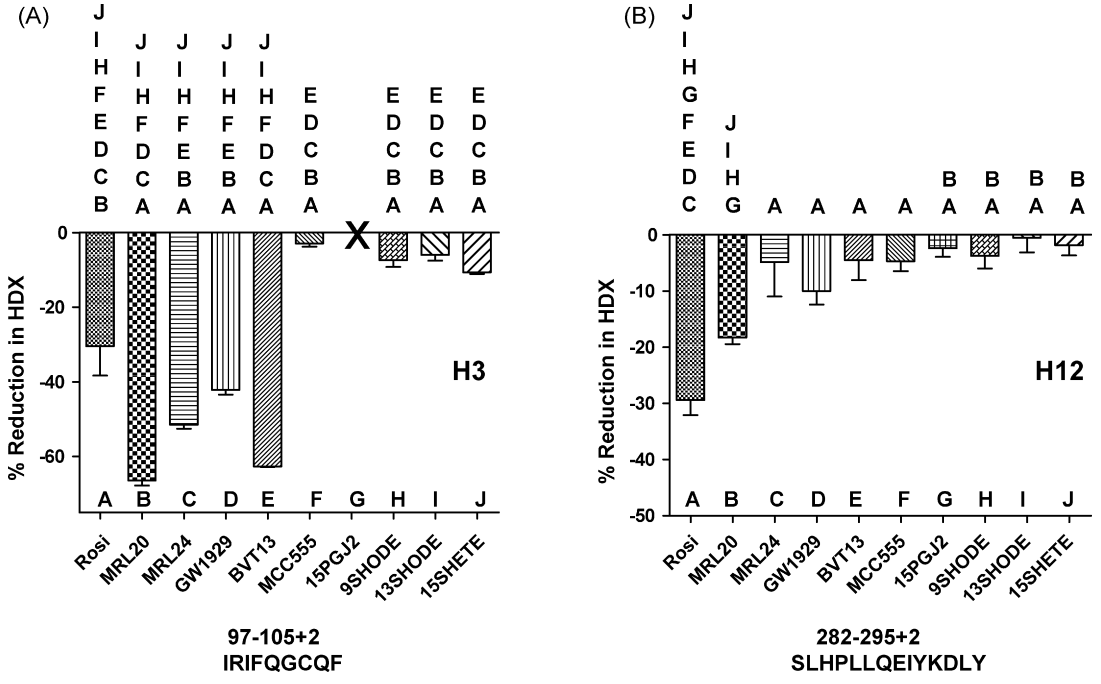

Fig. 3. Differential HDX data for the H3 (A) and H12 (B) regions of the PPARγ LBD. Annotations to the bar chart correspond to the results from a Tukey multiple comparison test ($P < 0.05$). Rosi, MRL20, MRL24, GW1929, BVT13 and MCC555 are synthetic PPARγ modulators. 15PGJ2, 9SHODE, 13SHODE, 15SHETE are putative endogenous ligands.

3.2. Tukey multiple comparison procedure.

The β-sheet region of PPARγ LBD has been implicated in a novel helix 12-independent mode of activation of the receptor [12]. Therefore the changes in HDX kinetics for this region upon ligand interaction are of interest. To establish the statistical significance of changes in HDX in this region for each ligand we employed a one way analysis of variance (optional) in conjunction with the Tukey multiple comparison procedure (Prism v5.0) in a fashion similar to that described by Hsu et al. [11] Results from this analysis are given in Table 2. In a pair wise fashion, ligands are compared and a *P*-value obtained. Annotation of Fig. 2(B) illustrates ligands that have significant differences in differential HDX kinetics ($P < 0.05$) as compared to each other from those pairs that do not demonstrate significance. For example ligand "A" (rosiglitazone) was significantly different from ligands B, C, D, E but not F, G, H, I, J. It should be noted that although the Tukey comparison provides a cross comparison of all 10 ligands, a much larger dataset is generated. From this dataset comprised of 10 ligands there are 45 comparisons (9 + 8 + 7 + 6 + 5 + 4 + 3 + 2 + 1) that must be performed (see Table 2). The results from the Tukey comparison for all peptides in the dataset are presented in Supplementary Table 1. This table illustrates the complexity of the expansion of the dataset (10 ligands and 28 peptides generate 1260 data points). It should also be noted that by presenting only the *P*-values from the cross comparison test crucial information on the direction of the change in HDX is lost. It may be shown that two ligands of interest are different, but is that change an increase or decrease in HDX kinetics? For the reasons outlined above, we choose to represent the results of the Tukey comparison data in combination with a histogram of the HDX data (Figs. 2(B) and 3).

3.3. Hierarchical cluster analysis.

We have demonstrated how heat maps in combination with hierarchical clustering can be used to classify and display differential HDX data obtained from the analysis of the estrogen receptor alpha (ERα) in complex with various SERMS [16]. The advantage of the heat map approach is it provides a condensed view that can be expanded to many hundreds of ligands. This is in contrast to a multiple comparison table (similar to that shown in Supplementary Table 1) which would expand to contain many thousands of comparisons. For example, the comparison of 100 ligands would yield 4950 results per peptide, or 138,600 data points for the PPARγ peptides shown in Table 1. The complete PPARγ HDX dataset has therefore been plotted as a heat map and is shown in Fig. 4. For this visualization we represent a reduction in HDX kinetics according to a blue color (For interpretation of the references to color in this figure, the reader is referred to the web version of the article.) gradient, and an increase in HDX kinetics according to a red colored gradient. The grey color represents no statistical significance ($P > 0.05$) in a two tailed *t*-test between the apo receptor DMSO only 30 s HDX data and the receptor/ligand complex 30 s HDX data. The inclusion of this *t*-test allows us to color only those regions that show a significant change and the blue/red color scheme maintains consistency across our HDX visualization components. Data were clustered according to Ward's method as described in Section 2.

Clearly the heat map provides a detailed overview of the screening dataset. When more detailed information is required for a specific region of the protein, the Tukey comparison annotated histogram of the peptide of interest should be consulted. When information is required for a specific ligand, a plot showing the %D change for all ligands across all peptides would provide additional information. Fig. 5 shows the HDX data plotted against all peptides in the dataset. The inclusion of error bars (standard errors, based on $n = 4$) provides for a visual representation of the precision of the measurements, a key feature of the data that cannot be represented on a heat map. As such we will incorporate all three of these graphical components into future versions of our HDX data analysis software.

Table 2
Tukey's multiple comparison test for PPARγ peptide $[159–169 + 2H]^{2+}$ (ISEGQFMTRE).

Comparison	Mean difference	$P < 0.05$?	Summary
Rosi vs MRL20	15.41	Yes	**
Rosi vs MRL24	18.86	Yes	***
Rosi vs GW1929	17.80	Yes	***
Rosi vs BVT13	33.54	Yes	***
Rosi vs MCC555	−9.080	No	ns
Rosi vs 15PGJ2	10.24	No	ns
Rosi vs 9SHODE	−10.31	No	ns
Rosi vs 13SHODE	−4.197	No	ns
Rosi vs 15SHETE	2.512	No	ns
MRL20 vs MRL24	3.453	No	ns
MRL20 vs GW1929	2.393	No	ns
MRL20 vs BVT13	18.13	Yes	***
MRL20 vs MCC555	−24.49	Yes	***
MRL20 vs 15PGJ2	−5.165	No	ns
MRL20 vs 9SHODE	−25.72	Yes	***
MRL20 vs 13SHODE	−19.61	Yes	***
MRL20 vs 15SHETE	−12.90	Yes	*
MRL24 vs GW1929	−1.060	No	ns
MRL24 vs BVT13	14.68	Yes	**
MRL24 vs MCC555	−27.94	Yes	***
MRL24 vs 15PGJ2	−8.618	No	ns
MRL24 vs 9SHODE	−29.17	Yes	***
MRL24 vs 13SHODE	−23.06	Yes	***
MRL24 vs 15SHETE	−16.35	Yes	**
GW1929 vs BVT13	15.74	Yes	**
GW1929 vs MCC555	−26.88	Yes	***
GW1929 vs 15PGJ2	−7.558	No	ns
GW1929 vs 9SHODE	−28.11	Yes	***
GW1929 vs 13SHODE	−22.00	Yes	***
GW1929 vs 15SHETE	−15.29	Yes	**
BVT13 vs MCC555	−42.62	Yes	***
BVT13 vs 15PGJ2	−23.30	Yes	***
BVT13 vs 9SHODE	−43.85	Yes	***
BVT13 vs 13SHODE	−37.74	Yes	***
BVT13 vs 15SHETE	−31.03	Yes	***
MCC555 vs 15PGJ2	19.32	Yes	***
MCC555 vs 9SHODE	−1.226	No	ns
MCC555 vs 13SHODE	4.883	No	ns
MCC555 vs 15SHETE	11.59	No	ns
15PGJ2 vs 9SHODE	−20.55	Yes	***
15PGJ2 vs 13SHODE	−14.44	Yes	*
15PGJ2 vs 15SHETE	−7.733	No	ns
9SHODE vs 13SHODE	6.109	No	ns
9SHODE vs 15SHETE	12.82	Yes	*
13SHODE vs 15SHETE	6.708	No	ns

ns = not significant.
* $P < 0.05$.
** $P < 0.01$.
*** $P < 0.001$.

3.4. HDX data provides new information about the PPARγ LBD.

Fig. 3 shows the HDX data and Tukey comparison for two regions of the receptor implicated in the regulation of its activity. Helix three (Fig. 3(A)) is located in the center of the ligand binding pocket and interacts with many of the synthetic ligands. For example MRL20 is positioned closer to H3 than MRL24 (PDB:2Q59 and PDB:2Q5P, Bruning et al. Fig. 8 [12]) and is within contact distance of Ile281, Gly284, Cys285, Arg288 and Ala292 (numbering scheme according to full length PPARγ). The proximity of the ligand to H3 results in a marked decrease in HDX kinetics (a reduction of 66% ± 3 from the apo value (87% ± 4)). MRL24 which is located further from H3 in the X-ray structure, reduced the dynamics of the receptor by 51% (±2). This change between the two ligands is significant

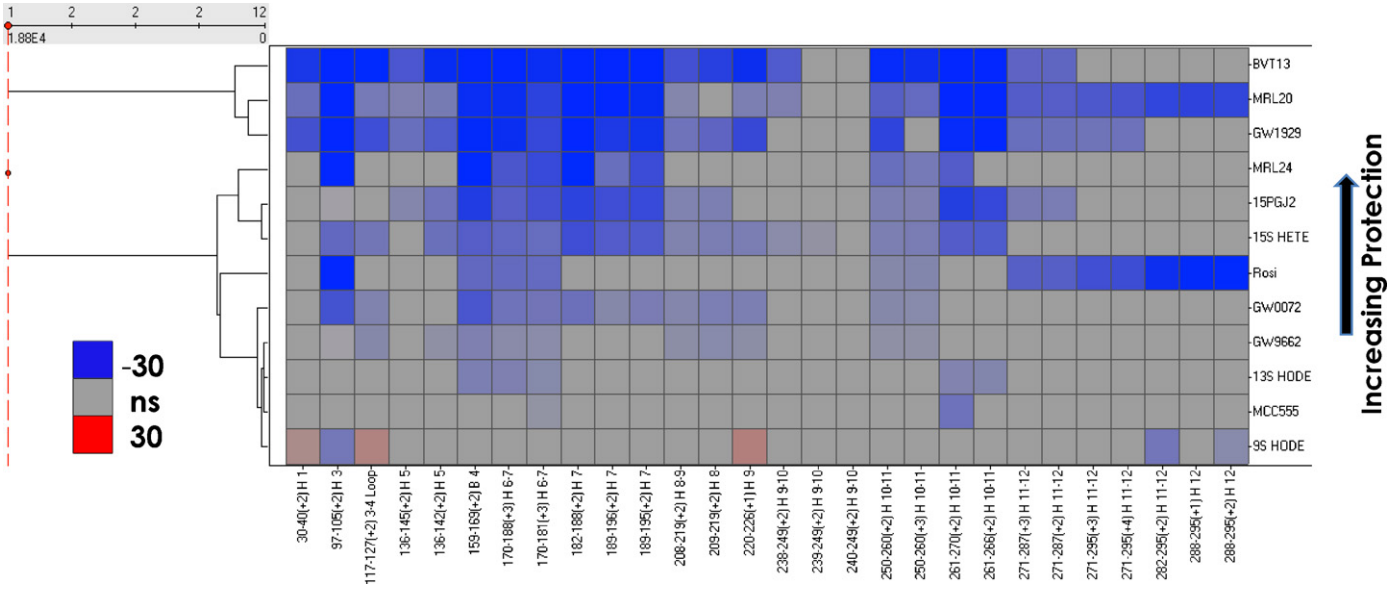

Fig. 4. Heat map of differential HDX data for PPARγ LBD. Changes with Tukey-adjusted *P*-values < 0.05 are colored according to the key. *P*-values > 0.05 are colored grey.

in the Tukey comparison (<0.05). These data highlight the ability of the HDX data to reflect changes in ligand binding within the receptor. It is apparent from Fig. 3(A) that none of the putative endogenous agonists of the receptor perturb the dynamics of H3 to the same extent as the synthetic ligands. No data could be obtained for 15PGJ2 which is a known to form a covalent bond to cysteine residue 103 of the receptor (Cys307 in full length PPARγ).

Helix 12 (H12) has been described as the "master switch" of nuclear receptors including PPARγ [44]. H12 along with H3–H4 loop comprise the so-called AF-2 (activation function-2) coacti-

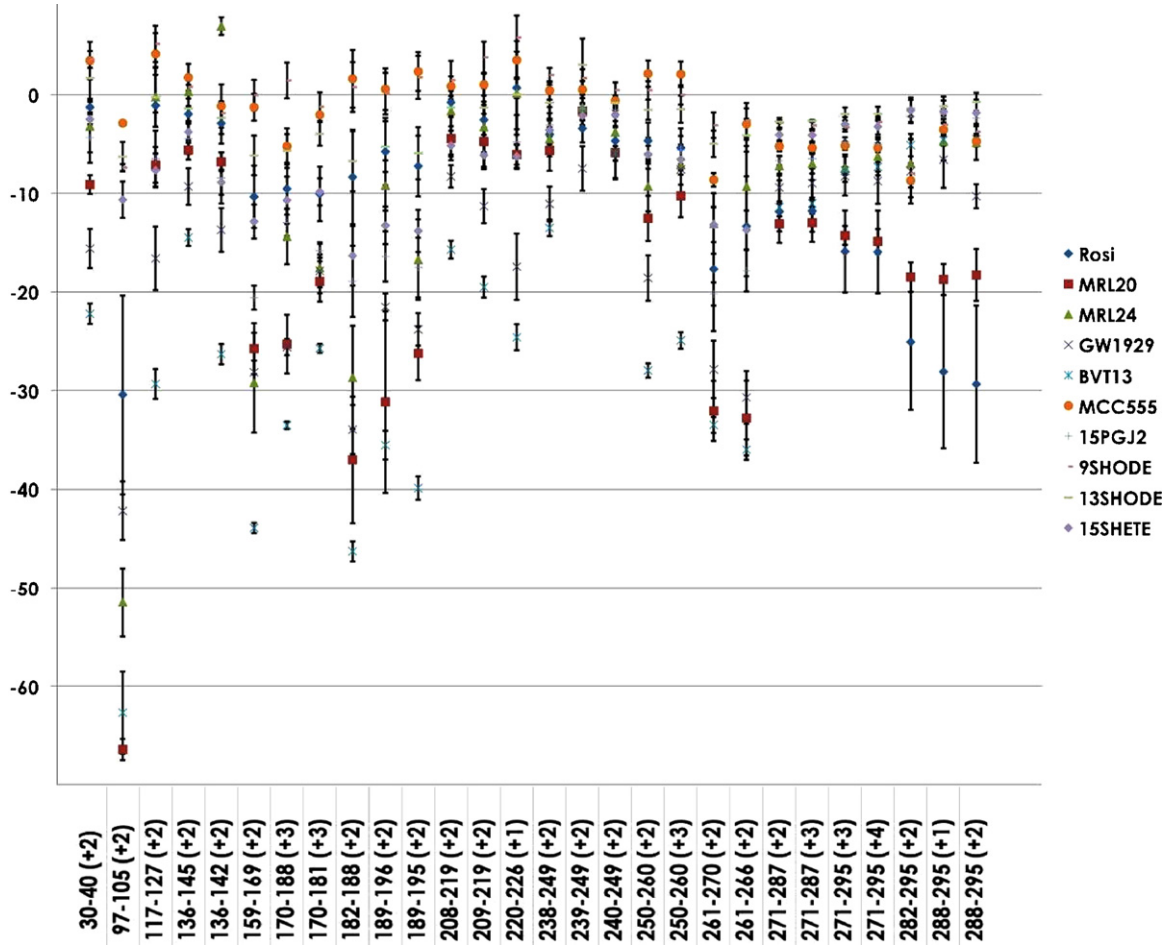

Fig. 5. Differential HDX data for PPARγ LBD with 10 ligands.

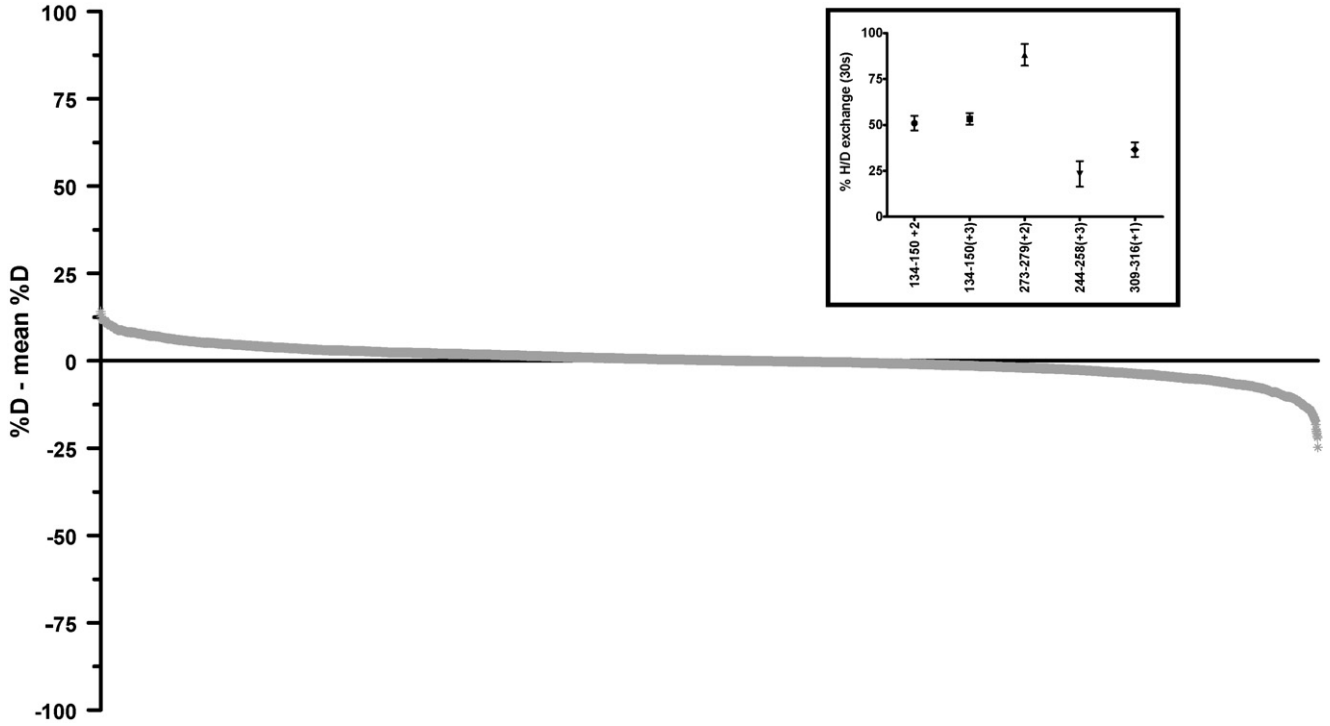

Fig. 6. Precision of the VDR LBD 30 s HDX experiment over an eight month time period. The inset to the figure shows the mean and standard deviation for five peptides calculated from 127 replicate analysis. The peptide spanning residues 134–150 was measured to have a mean %D value of 51%D and a standard deviation of 3.7. The main panel to the figure plots the difference of each replicate from the mean (33 peptides × 127 replicates = 4191 values). Data are ordered from high to low values. 96% of all values are within 10% of the mean.

vator binding site. Deletions of H12 or the point mutation Y473A (position in the full length PPARγ sequence) renders the PPARγ silent to full agonists. Previous studies we have shown that full agonists reduced HDX kinetics of the AF-2 surface. Thus, HDX analysis is sensitive not only to binding, but to reading out dynamics that can have a direct impact on receptor function. The HDX data for H12 are shown in Fig. 3(B). As expected, the most significant reduction in HDX was observed for the synthetic agonist rosiglitazone.

Although the visualization of the data in Supplementary Table 1 are somewhat difficult due to the large number of data points displayed, results for the peptide spanning residues 239–249 (LKLNHPESSQL $[M+2H]^{2+}$) stand out because there are no statistically significant changes in this region (H9–H10 link). Therefore, for this set of ligands, the dynamics of this region of the receptor can be determined to be totally insensitive to ligand binding. This is the only region of the receptor that exhibits this behavior.

3.5. Appraising the quality of the HDX MS platform

To evaluate the workflow described above with a larger dataset and to assess the precision of our system we have focused on a set of experiments performed with the vitamin D receptor (VDR). We have a significant ongoing effort to profile the HDX fingerprint of VDR ligands, including small molecules, fragments, cofactor proteins and DNAs. Because all the data are readily accessible from the relational database, we extracted the differential HDX data for 40 VDR ligands acquired over an eight month time period. Each VDR experiment contained data for 34 different peptides and total 4191 discrete %D values. In order to maintain the quality of our data, each experiment contained a DMSO internal control and all were acquired with the same orbitrap mass spectrometer. Subsequent to acquisition all mass spectral data were visually inspected to assess the quality of the measured isotopic distribution. The manual inspection is time-consuming, however we believe this is an

Table 3
Data from 40 replicate HDX experiments acquired over an eight month time period. Values provided are the mean and standard deviation values obtained from 127 replicates.

Peptide	Mean	Standard deviation
134–150(+2)	51	3.7
134–150(+3)	53	3.2
219–224(+1)	106	7.3
225–233(+1)	74	6.7
225–233(+2)	92	5.8
234–244(+2)	62	4.4
244–258(+3)	23	6.9
244–259(+2)	27	2.2
245–258(+3)	27	6.0
245–259(+2)	30	2.5
273–279(+2)	88	5.9
274–285(+2)	85	6.2
286–308(+3)	87	4.7
300–308(+2)	87	5.6
309–316(+1)	37	4.0
309–316(+2)	40	3.6
309–325(+3)	43	4.8
309–329(+3)	37	3.9
309–333(+3)	27	3.3
317–325(+2)	50	6.0
317–329(+2)	40	4.1
336–351(+2)	34	2.4
338–351(+2)	43	2.9
352–365(+2)	3	0.5
354–365(+2)	3	1.1
366–379(+2)	39	2.7
366–379(+3)	39	2.6
366–383(+3)	33	2.3
366–383(+4)	34	2.5
384–389(+2)	3	1.3
384–390(+2)	3	0.8
384–403(+3)	53	3.8
384–403(+4)	54	3.9
390–403(+2)	72	5.3

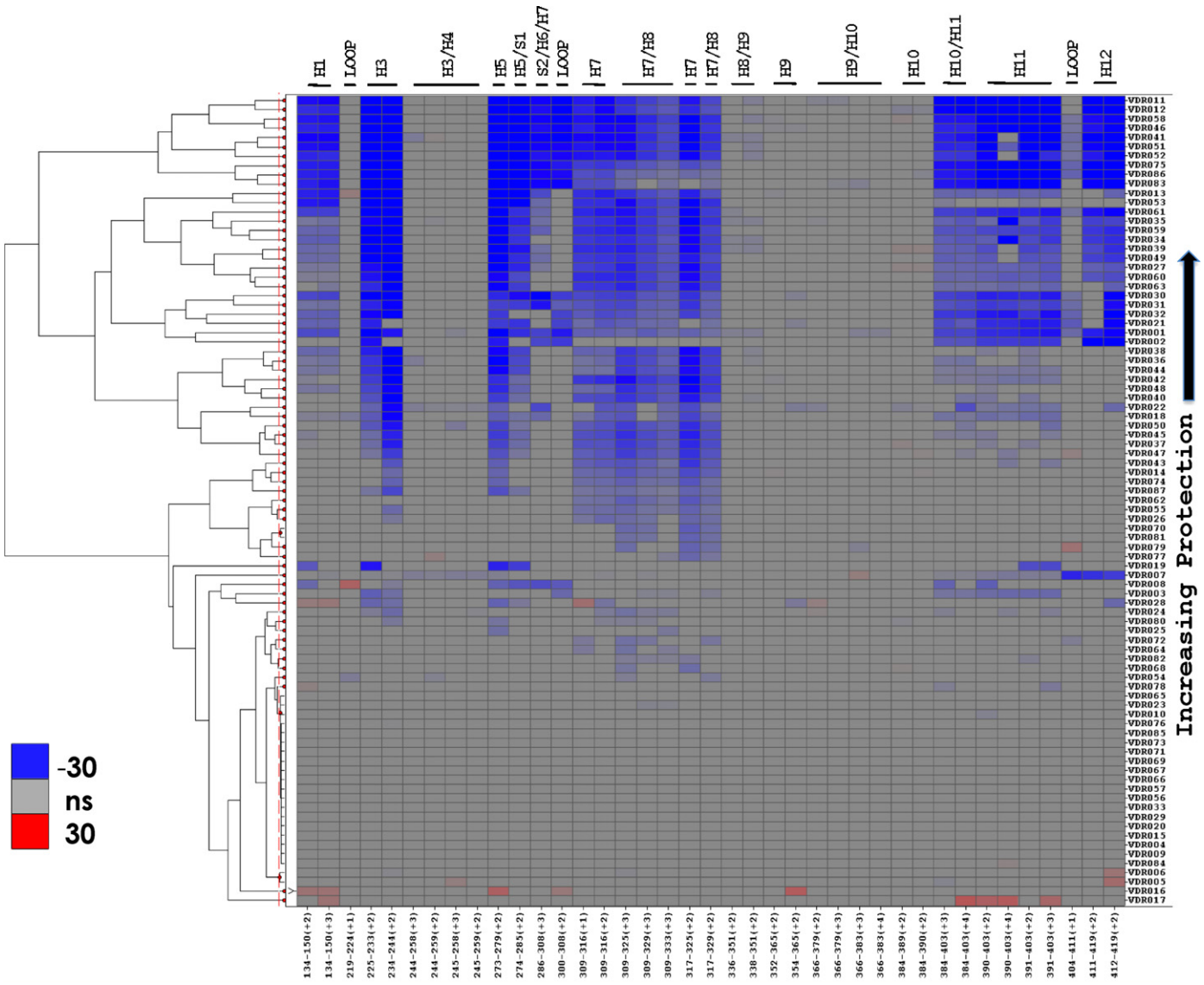

Fig. 7. HDX heat map obtained from the analysis of VDR LBD in complex with 87 ligands of interest. Data are clustered and ordered according the methods table. Changes with Tukey-adjusted *P*-values < 0.05 are colored according to the key. *P*-values > 0.05 are colored grey.

important part of the QC process for HDX data analysis (at least until the reliability of fully automated approaches are demonstrated on a manually verified dataset of a similar complexity). From these data we can assess the performance of our HDX platform over a significant period of time.

The acquisition of the DMSO control with each experiment provides us with many replicate analyses of the same protein acquired under the same HDX and MS conditions. To evaluate the quality of our HDX data we determined the mean %D value for 34 peptides across the 40 HDX experiments (127 total %D measurements for each peptide) and the results are given in Table 3. The inset to Fig. 6 shows the mean and standard deviation for five of these peptides following 30 s of on-exchange ($n = 127$). The peptide spanning residues 134–150 ($[M+2H]^{2+}$ ion) gave a mean % HDX value of 51 and a standard deviation of only 3.7%. An alternate way to display the precision of the data is to plot the distance of these measured values from the mean values. Fig. 6 shows all 4191 measurements (measured %D – mean %D for all 34 peptides (4191 values)) ordered from largest to smallest values. The data illustrate the precision of these replicate HDX experiments. It was determined that 4039 values were within 10% of the measured mean (>96%) and 3452 were within 5% of the mean (82%). These data show our ability to acquire HDX MS data with high precision over a significant period of time, and therefore validates our large scale cross comparison of multiple HDX datasets.

Having established that our HDX system can operate with high precision over significant periods of time, we performed the cross comparison of 87 HDX datasets acquired over a two-year period. The data were treated as described in Sections 3.2 and 3.3. The heat map and cluster analysis are shown in Fig. 7. This figure summarizes by far the largest single HDX experiment published to date and the acquisition and analysis of the data are ongoing.

4. Conclusions

We have outlined a data analysis workflow for integration into our HDX software and a schematic representation of this workflow is shown in Fig. 1. We validated the approach with a small dataset of 10 PPARγ ligands. Data are compared with a Tukey cross comparison test and statistically significant changes are plotted in a heat map. The performance of our HDX system was then evaluated

with a dataset comprised of 40 differential HDX experiments. The precision of the data exceeded our expectations. For example, over an eight month period 127 replicate measurements of the 134–150 $[M+2H]^{2+}$ peptide yielded an mean of 51%D with a standard deviation of only 3.7%. Having established the precision of the system for an additional 36 peptides we determined that over 96% of our measured %D values were within 10% of their mean values. Finally we show the differential HDX data for 87 ligands acquired over a two-year period. Together we show how subtle, but statistically significant changes in HDX data can be used to probe the mechanism of action for synthetic and endogenous ligands of interest.

Acknowledgements

This work was supported in part by the Intramural Research Program of the National Institutes of Health National Institute of Mental Health [Grant U54-MH074404] and by the National Institutes of Health National Institute of General Medical Sciences [Grant R01-GM084041].

Appendix A. Supplementary data

Supplementary data associated with this article can be found, in the online version, at doi:10.1016/j.ijms.2010.08.002.

References

[1] J.R. Engen, Analysis of protein conformation and dynamics by hydrogen/deuterium exchange MS, Anal. Chem. 81 (19) (2009) 7870–7875.
[2] J.R. Engen, D.L. Smith, Investigating protein structure and dynamics by hydrogen exchange MS, Anal. Chem. 73 (9) (2001) 256a–265a.
[3] S.W. Englander, Hydrogen exchange and mass spectrometry: a historical perspective, J. Am. Soc. Mass Spectrom. 17 (11) (2006) 1481–1489.
[4] X. Yan, C.S. Maier, Hydrogen/deuterium exchange mass spectrometry, Methods Mol. Biol. 492 (2009) 255–271.
[5] I.A. Kaltashov, C.E. Bobst, R.R. Abzalimov, H/D exchange and mass spectrometry in the studies of protein conformation and dynamics: is there a need for a top-down approach? Anal. Chem. 81 (19) (2009) 7892–7899.
[6] P.S. Chetty, L. Mayne, S. Lund-Katz, D. Stranz, S.W. Englander, M.C. Phillips, Helical structure and stability in human apolipoprotein A-I by hydrogen exchange and mass spectrometry, Proc Natl Acad Sci U. S. A. 106 (2009) 19005–19010.
[7] K.S. Gajiwala, J.C. Wu, J. Christensen, G.D. Deshmukh, W. Diehl, J.P. DiNitto, J.M. English, M.J. Greig, Y.A. He, S.L. Jacques, E.A. Lunney, M. McTigue, D. Molina, T. Quenzer, P.A. Wells, X. Yu, Y. Zhang, A. Zou, M.R. Emmett, A.G. Marshall, H.M. Zhang, G.D. Demetri, KIT kinase mutants show unique mechanisms of drug resistance to imatinib and sunitinib in gastrointestinal stromal tumor patients, Proc Natl Acad Sci U S A 106 (2009) 1542–1547.
[8] J.R. Horn, B. Kraybill, E.J. Petro, S.J. Coales, J.A. Morrow, Y. Hamuro, A.A. Kossiakoff, The role of protein dynamics in increasing binding affinity for an engineered protein-protein interaction established by H/D exchange mass spectrometry, Biochemistry 45 (2006) 8488–8498.
[9] I. Gertsman, E.A. Komives, J.E. Johnson, HK97 maturation studied by crystallography and H/2H exchange reveals the structural basis for exothermic particle transitions, J. Mol. Biol. 397 (2) (2010) 560–574.
[10] D. Houde, J. Arndt, W. Domeier, S. Berkowitz, J.R. Engen, Characterization of IgG1 Conformation and Conformational Dynamics by Hydrogen/Deuterium Exchange Mass Spectrometry, Analytical Chemistry 81 (2009) 2644–2651.
[11] Y.H. Hsu, D.A. Johnson, J.A. Traugh, Analysis of conformational changes during activation of protein kinase Pak2 by amide hydrogen/deuterium exchange, J. Biol. Chem. 283 (52) (2008) 36397–36405.
[12] J.B. Bruning, M.J. Chalmers, S. Prasad, S.A. Busby, T.M. Karnenecka, Y.J. He, K.W. Nettles, P.R. Griffin, Partial agonists activate PPAR gamma using a helix 12 independent mechanism, Structure 15 (2007) 1258–1271.
[13] M.J. Chalmers, S.A. Busby, B.D. Pascal, Y.J. He, C.L. Hendrickson, A.G. Marshall, P.R. Griffin, Probing protein ligand interactions by automated hydrogen/deuterium exchange mass spectrometry, Anal. Chem. 78 (2006) 1005–1014.
[14] M.J. Chalmers, S.A. Busby, B.D. Pascal, M.R. Southern, P.R. Griffin, A two-stage differential hydrogen deuterium exchange method for the rapid characterization of protein/ligand interactions, J. Biomol. Tech. 18 (2007) 194–204.
[15] S.Y. Dai, T.P. Burris, J.A. Dodge, C. Montrose-Rafizadeh, Y. Wang, B.D. Pascal, M.J. Chalmers, P.R. Griffin, Unique ligand binding patterns between estrogen receptor alpha and beta revealed by hydrogen-deuterium exchange, Biochemistry-Us 48 (2009) 9668–9676.
[16] S.Y. Dai, M.J. Chalmers, J. Bruning, K.S. Bramlett, H.E. Osborne, C. Montrose-Rafizadeh, R.J. Barr, Y. Wang, M.M. Wang, T.P. Burris, J.A. Dodge, P.R. Griffin, Prediction of the tissue-specificity of selective estrogen receptor modulators by using a single biochemical method, Proc. Natl. Acad. Sci. U.S.A. 105 (2008) 7171–7176.
[17] Y. Hamuro, S.J. Coales, J.A. Morrow, K.S. Molnar, S.J. Tuske, M.R. Southern, P.R. Griffin, Hydrogen/deuterium-exchange (H/D-Ex) of PPARgamma LBD in the presence of various modulators, Protein Sci. 15 (2006) 1883–1892.
[18] X. Yan, D. Broderick, M.E. Leid, M.I. Schimerlik, M.L. Deinzer, Dynamics and ligand-induced solvent accessibility changes in human retinoid X receptor homodimer determined by hydrogen deuterium exchange and mass spectrometry, Biochemistry-Us 43 (2004) 909–917.
[19] X. Yan, M.L. Deinzer, M.I. Schimerlik, D. Broderick, M.E. Leid, M.I. Dawson, Investigation of ligand interactions with human RXRalpha by hydrogen/deuterium exchange and mass spectrometry, J. Am. Soc. Mass Spectrom. 17 (2006) 1510–1517.
[20] X. Yan, E. Perez, M. Leid, M.I. Schimerlik, A.R. de Lera, M.L. Deinzer, Deuterium exchange and mass spectrometry reveal the interaction differences of two synthetic modulators of RXRalpha LBD, Protein Sci. 16 (2007) 2491–2501.
[21] X.G. Yan, D. Broderick, M.E. Leid, M.I. Schimerlik, M.L. Deinzer, Dynamics and ligand-induced solvent accessibility changes in human retinoid X receptor homodimer determined by hydrogen deuterium exchange and mass spectrometry, Biochemistry 43 (2004) 909–917.
[22] A.A. Edwards, J.D., Tipton, M.D. Brenowitz, M.R., Emmett, A.G. Marshall, G.B., Evans, P.C. Tyler, V.L. Schramm, Conformational states of human purine nucleoside phosphorylase at rest, at work, and with transition state analogues, Biochemistry 49(9) (2010), 2058–2067.
[23] V. Chandra, P. Huang, Y. Hamuro, S. Raghuram, Y. Wang, T.P. Burris, F. Rastinejad, Structure of the intact PPAR-gamma-RXR-alpha nuclear receptor complex on DNA, Nature (2008) 350–356.
[24] G. Spraggon, D. Pantazatos, H.E. Klock, I.A. Wilson, V.L. Woods Jr., S.A. Lesley, On the use of DXMS to produce more crystallizable proteins: structures of the *T. maritima* proteins TM0160 and TM1171, Protein Sci. 13 (2004) 3187–3199.
[25] D. Pantazatos, J.S. Kim, H.E. Klock, R.C. Stevens, I.A. Wilson, S.A. Lesley, V.L. Woods Jr., Rapid refinement of crystallographic protein construct definition employing enhanced hydrogen/deuterium exchange MS, Proc. Natl. Acad. Sci. U.S.A. 101 (2004) 751–756.
[26] X. Zhang, E.Y.T. Chien, M.J. Chalmers, B.D. Pascal, J. Gatchalian, R.C. Stevens, P.R. Griffin, Dynamics of the beta(2)-Adrenergic G-Protein Coupled Receptor Revealed by Hydrogen-Deuterium Exchange, Anal. Chem. 82 (2010) 1100–1108.
[27] N.H. Joh, A. Min, S. Faham, J.P. Whitelegge, D. Yang, V.L. Woods, J.U. Bowie, Modest stabilization by most hydrogen-bonded side-chain interactions in membrane proteins, Nature 453 (2008) 1266–1270.
[28] L.S. Busenlehner, J. Alander, C. Jegerscohld, P.J. Holm, P. Bhakat, H. Hebert, R. Morgenstern, R.N. Armstrong, Location of substrate binding sites within the integral membrane protein microsomal glutathione transferase-1, Biochemistry 46 (2007) 2812–2822.
[29] L.S. Busenlehner, G. Branden, I. Namslauer, P. Brzezinski, R.N. Armstrong, Structural elements involved in proton translocation by cytochrome c oxidase as revealed by backbone amide hydrogen-deuterium exchange of the E286H mutant, Biochemistry 47 (2008) 73–83.
[30] L.S. Busenlehner, L. Salomonsson, P. Brzezinski, R.N. Armstrong, Mapping protein dynamics in catalytic intermediates of the redox-driven proton pump cytochrome c oxidase, Proc. Natl. Acad. Sci. U.S.A. 103 (2006) 15398–15403.
[31] Y. Hamuro, S.J. Coales, M.R. Southern, J.F. Nemeth-Cawley, D.D. Stranz, P.R. Griffin, Rapid analysis of protein structure and dynamics by hydrogen/deuterium exchange mass spectrometry, J. Biomol. Tech. 14 (2003) 171–182.
[32] M. Hotchko, G.S. Anand, E.A. Komives, L.F. Ten Eyck, Automated extraction of backbone deuteration levels from amide H/2H mass spectrometry experiments, Protein Sci. 15 (2006) 583–601.
[33] M. Palmblad, J. Buijs, P. Hakansson, Automatic analysis of hydrogen/deuterium exchange mass spectra of peptides and proteins using calculations of isotopic distributions, J. Am. Soc. Mass Spectrom. 12 (2001) 1153–1162.
[34] D.D. Weis, J.R. Engen, I.J. Kass, Semi-automated data processing of hydrogen exchange mass spectra using HX-Express, J. Am. Soc. Mass Spectrom. 17 (12) (2006) 1700–1703.
[35] B.D. Pascal, M.J. Chalmers, S.A. Busby, P.R. Griffin, HD desktop: an integrated platform for the analysis and visualization of H/D Exchange data, J. Am. Soc. Mass Spectr. 20 (2009) 601–610.
[36] B.D. Pascal, M.J. Chalmers, S.A. Busby, C.C. Mader, M.R. Southern, N.F. Tsinoremas, P.R. Griffin, The deuterator: software for the determination of backbone amide deuterium levels from H/D exchange MS data, Bmc. Bioinformatics 8 (2007) 156.
[37] S. Kazazic, H.M. Zhang, T.M. Schaub, M.R. Emmett, C.L. Hendrickson, G.T. Blakney, A.G. Marshall, Automated data reduction for hydrogen/deuterium exchange experiments, enabled by high-resolution Fourier transform ion cyclotron resonance mass spectrometry, J. Am. Soc. Mass Spectrom. 21 (4) (2010) 550–558.
[38] G.W. Slysz, C.A.H. Baker, B.M. Bozsa, A. Dang, A.J. Percy, M. Bennett, D.C. Schriemer, Hydra: software for tailored processing of H/D exchange data from MS or tandem MS analyses, Bmc. Bioinformatics 10 (2009).
[39] P. Nikamanon, E. Pun, W. Chou, M.D. Koter, P.D. Gershon, TOF2H": A precision toolbox for rapid, high density/high coverage hydrogen-deuterium exchange mass spectrometry via an LC-MALDI approach, covering the data pipeline from spectral acquisition to HDX rate analysis, Bmc. Bioinformatics 9 (2008).
[40] X. Lou, M. Kirchner, B.Y. Renard, U. Köthe, S. Boppel, C. Graf, C.-T. Lee, J.A.J. Steen, H. Steen, M.P. Mayer, A. Fred, Hamprecht deuteration distribution estimation

with improved sequence coverage for HX/MS experiments, Bioinformatics 26 (12) (2010) 1535–1541.
[41] K. Juntunen, N. Rochel, D. Moras, P. Vihko, Large-scale expression and purification of the human vitamin D receptor and its ligand-binding domain for structural studies, Biochem. J. 344 (2 Pt) (1999) 297–303.
[43] J.H. Ward, Hierarchical grouping to optimize an objective function, J. Am. Stat. Assoc. 58 (301) (1963) 236–244.
[44] K.W. Nettles, G.L. Greene, Ligand control of coregulator recruitment to nuclear receptors, Annu. Rev. Physiol. 67 (2005) 309–333.